

Graphical Abstract

Topological Percolation in Urban Dengue Transmission: A Multi-Scale Analysis of Spatial Connectivity

Marcílio Ferreira dos Santos, Cleiton de Lima Ricardo

Highlights

Topological Percolation in Urban Dengue Transmission: A Multi-Scale Analysis of Spatial Connectivity

Marcílio Ferreira dos Santos, Cleiton de Lima Ricardo

- We study the spatial organization of urban dengue cases using a percolation-based topological framework grounded in zero-dimensional persistent homology.
- Spatial connectivity is analyzed through Vietoris–Rips filtrations parametrized by percentiles of the empirical distance distribution, enabling scale-free comparison across years.
- Distinct percolation regimes are identified, ranging from fragmented spatial patterns to highly concentrated, percolated structures.
- Years with similar incidence levels exhibit markedly different percolation behavior, demonstrating that case counts alone do not determine epidemic spatial structure.
- A pronounced structural rupture is observed in 2020, characterized by delayed or absent spatial percolation, consistent with altered urban mobility.

Topological Percolation in Urban Dengue Transmission: A Multi-Scale Analysis of Spatial Connectivity

Marcílio Ferreira dos Santos^{a,b}, Cleiton de Lima Ricardo^{b,1}

^aNúcleo de Formação de Docentes, Universidade Federal de Pernambuco (UFPE), , Caruaru, , PE, Brazil

^bNúcleo Interdisciplinar de Ciências Exatas e da Natureza (NICEN), Universidade Federal de Pernambuco (UFPE), , Caruaru, , PE, Brazil

Abstract

We investigate the spatial organization of dengue cases in the city of Recife, Brazil, from 2015 to 2024, using tools from statistical physics and topological data analysis. Reported cases are modeled as point clouds in a metric space, and their spatial connectivity is studied through Vietoris–Rips filtrations and zero-dimensional persistent homology, which captures the emergence and collapse of connected components across spatial scales. By parametrizing the filtration using percentiles of the empirical distance distribution, we identify critical percolation thresholds associated with abrupt growth of the largest connected component. These thresholds define distinct geometric regimes, ranging from fragmented spatial patterns to highly concentrated, percolated structures. Remarkably, years with similar incidence levels exhibit qualitatively different percolation behavior, demonstrating that case counts alone do not determine the spatial organization of transmission. Our analysis further reveals pronounced temporal heterogeneity in the percolation properties of dengue spread, including a structural rupture in 2020 characterized by delayed or absent spatial percolation. These findings highlight percolation-based topological observables as physically interpretable and sensitive descriptors of urban epidemic structure, offering a complementary perspective to traditional spatial and epidemiological analyses.

Keywords: Topological Data Analysis; Persistent Homology; Geometric Percolation; Statistical Physics; Spatial Point Processes; Urban Epidemics; Dengue Transmission

1. Introduction

Dengue remains one of the most impactful vector-borne diseases worldwide, with estimates indicating approximately 390 million infections annually and recurrent outbreaks across tropical and subtropical regions. Its primary vector, *Aedes aegypti*, exhibits a strong dependence on urban spatial structure, operating predominantly over short distances and generating local transmission clusters whose fine-scale geometry is crucial for epidemiological surveillance [1, 2]. From a physical perspective, this dynamics suggests a spatial connectivity process governed by local interactions within a het-

erogeneous urban medium, in which macroscopic patterns emerge from restricted microscopic interactions.

Traditional epidemiological models, including compartmental frameworks and classical statistical approaches, describe aggregated trends but fail to recover the underlying geometry of transmission [4]. Even more sophisticated spatial models often rely on coarse administrative units, which can smooth out or mask local heterogeneities that play a central role in vector–host interactions. In terms of statistical physics, this limitation corresponds to a loss of structural information associated with local connectivity and the formation of spatial clusters.

Topological Data Analysis (TDA) provides a complementary perspective that is particularly well suited to this challenge. Rather than imposing predefined spatial partitions, TDA extracts multiscale geometric properties directly from the observed point cloud, quantifying connectivity, fragmentation, and the emergence of topological structures associated with spatial heterogeneity. Persistent homology, the core tool of TDA,

*Corresponding author.

Email addresses: marcilio.santos@ufpe.br (Marcílio Ferreira dos Santos), cleiton.lricardo@ufpe.br (Cleiton de Lima Ricardo)

URL: <https://orcid.org/0000-0001-8724-0899> (Marcílio Ferreira dos Santos), <https://orcid.org/0000-0002-7114-1201> (Cleiton de Lima Ricardo)

tracks the birth and death of these structures across filtration scales, producing invariants capable of summarizing complex patterns in a mathematically rigorous manner [5, 6, 7].

From the viewpoint of complex systems physics, the evolution of connectivity along the filtration scale can be interpreted as a geometric percolation process in a continuous spatial system, in which local connected components progressively merge until the emergence of a dominant cluster [8, 9]. Analogous processes have been widely studied in random geometric graphs, spatial networks, and urban systems, where the underlying geometry plays a central role in shaping global dynamics [11].

Although TDA has been successfully applied in areas such as disordered materials, complex networks, granular systems, neuroscience, and climate sciences [12], its systematic use in spatial epidemiology remains incipient. In particular, few studies explicitly explore the relationship between persistent homology, spatial percolation, and structural connectivity regimes in high-resolution urban epidemiological data.

The availability of street-level georeferenced dengue data in Recife creates an unprecedented opportunity to construct “epidemic shapes” directly from the distribution of reported cases. Rather than explicitly modeling transmission chains, we examine the geometry of the epidemic field over time. Using Vietoris–Rips complexes constructed from Euclidean metrics in urban metric coordinates, we analyze zero-dimensional persistent homology, associated with the spatial connectivity of cases, across epidemiologically plausible scales.

We show that the evolution of spatial connectivity among dengue cases exhibits abrupt transitions consistent with distinct percolation regimes, enabling the classification of the analyzed years into patterns of concentrated, diffuse, and multifocal transmission. In particular, we identify critical scales associated with the topological collapse of spatial fragmentation, as well as atypical years whose topological signatures differ substantially from classical epidemic regimes. These results demonstrate that persistent homology captures structural aspects of dengue spatial dynamics that remain invisible to traditional spatial statistical approaches.

More broadly, this work illustrates how tools from statistical physics, percolation theory, and algebraic topology can be integrated to provide a geometric and multiscale characterization of disease spread in complex urban environments, positioning Topological Data Analysis as a promising framework for the understanding of spatial epidemiological phenomena.

2. Materials and Methods

2.1. Epidemiological data and geocoding

We used confirmed dengue case data reported in the municipality of Recife, Brazil, between 2015 and 2024. Each record corresponds to an individual case associated with a street address or postal code (CEP), from which geographic coordinates were obtained using automated geocoding services. This procedure assigns each address to an approximate location along the corresponding street segment, typically near the centroid of the road axis [15].

It is well recognized that automated address geocoding does not provide the exact physical location of a residence, but rather an estimate based on interpolation along the street network. Classical studies in spatial epidemiology have shown that this type of geocoding introduces unavoidable positional error. In particular, comparisons between automatically geocoded coordinates and true address locations obtained via visual inspection of aerial imagery indicate that, in dense urban areas, the mean positional error is on the order of 50–60 m, and that approximately 95% of geocoded addresses lie within 150 m of their true locations [14].

Accordingly, the coordinates used in this study should be interpreted as approximate spatial representations subject to positional uncertainty. While this limitation may affect the precise location of individual cases, it does not invalidate the analysis of collective and multiscale spatial patterns, particularly those based on topological connectivity, which are known to be stable under small perturbations of the underlying point cloud.

2.2. Coordinate system and spatial metric

To ensure metric consistency in the spatial analyses, all geographic coordinates were projected into the SIRGAS 2000 / UTM Zone 25S coordinate system, allowing distances to be expressed directly in meters. The Euclidean distance in the projected plane was adopted as the spatial metric, serving as an effective approximation of geographic proximity between cases at the urban scale.

More complex metrics, such as network-constrained distances along the street network or anisotropic metrics induced by urban morphology, were not considered in this version of the study. Assessing the impact of alternative distance measures on topological connectivity constitutes a natural direction for future work.

2.3. Point cloud representation and Vietoris–Rips complexes

For each year analyzed, dengue cases were represented as a spatial point cloud

$$D = \{x_1, x_2, \dots, x_N\} \subset \mathbb{R}^2,$$

where each point x_i corresponds to the geocoded location of a reported case in the urban plane.

From this point cloud, a geometric graph parametrized by a connectivity radius $\varepsilon > 0$ was constructed, in which two points x_i and x_j are connected by an edge whenever the Euclidean distance satisfies $\|x_i - x_j\| \leq \varepsilon$. The Vietoris–Rips complex $VR(\varepsilon)$ is defined as the clique complex associated with this graph, such that any set of $k + 1$ mutually connected vertices defines a k -simplex.

The continuous variation of the parameter ε induces an increasing filtration of simplicial complexes,

$$VR(\varepsilon_1) \subseteq VR(\varepsilon_2), \quad \varepsilon_1 < \varepsilon_2,$$

which describes the multiscale evolution of spatial connectivity among cases.

2.4. Zero-dimensional persistent homology

In this work, the analysis focuses on zero-dimensional persistent homology (H_0), which captures exclusively the connectivity structure of the system. Each H_0 class corresponds to a connected component of the complex, whose birth occurs when a point appears in isolation, and whose death corresponds to the merging of that component with another as the parameter ε increases.

The evolution of H_0 classes along the filtration provides a multiscale description of the coalescence process among spatial clusters, allowing the identification of fragmented regimes, intermediate phases, and the collapse of connectivity into a dominant component, without imposing administrative partitions or explicit parametric models.

2.5. Topological observables and identification of transitions

For each value of ε , the following structural observables were extracted:

- the total number of connected components $N_c(\varepsilon)$;
- the size of the largest connected component $S_{\max}(\varepsilon)$;
- the distribution of sizes of intermediate components.

The critical connectivity scale $\varepsilon_{\text{crit}}$ was identified operationally as the value of ε associated with the largest discrete negative variation of $N_c(\varepsilon)$ along the filtration, corresponding to the most abrupt structural reorganization of spatial connectivity. This behavior is interpreted as an empirical transition analogous to a geometric percolation process in finite spatial systems.

2.6. Analyzed spatial scales

The Vietoris–Rips filtration was performed for values of ε ranging from 100 m to 500 m, with increments of 10 m. This interval was selected based on epidemiological and urban considerations, reflecting the limited mobility of the *Aedes aegypti* vector and the typical organization of urban space into blocks and micro-neighborhoods.

This multiscale sweep enables the identification of regions of topological stability, as well as abrupt transitions in connectivity, without imposing a priori a privileged spatial scale.

2.7. Considerations on null models

In the present version of the study, no systematic comparison with spatial null models was performed, such as random point distributions constrained to the urban support. Although such models are relevant for assessing the extent to which the observed topological signatures exceed those expected from urban geometry alone, this analysis is beyond the scope of the current version (arXiv) and will be addressed in future work.

3. Percolation structure and interpretation in finite systems

Percolation theory provides a fundamental conceptual framework for understanding emergent connectivity phenomena in spatial systems. Although originally developed in the context of ideal disordered media and infinite networks, its core principles have been extensively employed to interpret structural transitions in finite and empirical systems, including geometric networks and real spatial processes.

In a geometric setting, percolation refers to the emergence of large-scale connectivity as the interaction radius between spatially embedded points is progressively increased.

Definition 1 (Geometric percolation). *Given a finite set of points embedded in a metric space, geometric percolation denotes the emergence of a macroscopic connected component as the interaction radius ε between*

points increases. This phenomenon is typically associated with abrupt changes in observables related to the global connectivity of the system.

Classical results on random geometric graphs show that, even in purely random spatial configurations, global connectivity does not arise gradually. Instead, it emerges through a relatively abrupt transition associated with a critical interaction scale. Below this scale, the system is dominated by small, disconnected components; above it, a dominant component appears, concentrating a significant fraction of the vertices.

In the theory of infinite systems, percolation is characterized by the existence of a unique infinite connected component above a critical threshold, with probability one. While this result does not apply literally to finite systems, it motivates the use of the largest connected component as a dominant structural observable in empirical analyses. In real spatial systems, the transition toward a percolating regime is therefore expected to manifest as a rapid and concentrated growth of the largest component, accompanied by a sharp reduction in the total number of connected components. This form of structural dominance provides a clear empirical signature of nontrivial spatial organization.

For finite systems, such as urban or epidemiological datasets, no phase transition exists in the strict sense of the thermodynamic limit. Nevertheless, statistical physics establishes that finite systems exhibit *percolation signatures*, expressed as rapid, though smooth, variations in connectivity observables as a control parameter is varied. These finite-size signatures are widely used to identify behaviors analogous to percolation in empirical data, particularly when the system is strongly constrained by geometric or spatial structure, as is the case in urban environments.

Within this framework, an operational definition of an empirical percolation scale can be introduced.

Definition 2. Definition (Empirical percolation scale). Let $N(\varepsilon)$ denote the number of connected components of the Vietoris–Rips complex constructed from the point set for a given value of ε . The empirical percolation scale ε^* is defined as the value of ε associated with the largest negative variation of $N(\varepsilon)$ along the filtration.

This quantity provides an operational estimate of the scale at which the most intense structural reorganization of the system occurs, acting as an empirical order parameter for geometric percolation in finite datasets. Moreover, the global shape of the fusion curve $N(\varepsilon)$ can be interpreted as an aggregate indicator of the system’s connectivity dynamics, enabling systematic comparisons across different spatial and temporal regimes.

4. Topological Analysis of the Spatial Distribution of Dengue Cases (2015–2024)

4.1. Construction of topological indicators

In this section, we analyze the spatial structure of dengue cases in the city of Recife between 2015 and 2024 using tools from Topological Data Analysis (TDA), with a focus on zero-dimensional persistent homology (H_0), which captures spatial connectivity among georeferenced case records. This approach enables a multiscale characterization of transmission patterns, going beyond purely aggregated metrics, density maps, or local spatial autocorrelation analyses.

The analysis is based on the construction of Vietoris–Rips complexes from the geographic coordinates of reported cases, using the Euclidean metric in a projected coordinate system (UTM) to ensure metric consistency across the spatial scales considered. Filtrations were performed for values of ε ranging from 100 m to 500 m, an interval compatible with epidemiologically plausible scales of indirect spatial interaction, local mobility, and urban neighborhood structure.

Table 1 summarizes the main topological indicators extracted for each year, including:

- (i) the total number of points (N), corresponding to the number of unique reported cases;
- (ii) the critical scale $\varepsilon_{\text{crit}}$, defined as the value of ε associated with the most abrupt growth of the largest connected component along the filtration;
- (iii) the size of the largest connected component at $\varepsilon = 300$ m;
- (iv) the number of connected components at this scale;
- (v) the maximum number of intermediate components observed throughout the filtration process;
- (vi) the collapse scale $\varepsilon_{\text{collapse}}$, defined as the smallest value of ε for which the largest component contains at least 50% of the points.

In addition to the summarized indicators, Fig. ?? shows the evolution of the number of connected components along the Vietoris–Rips filtration for each analyzed year. The curves reveal distinct patterns of spatial connectivity reorganization, allowing direct visualization of the formation of dominant components and the emergence of contrasting topological regimes over the study period. Structural similarities among subsets of these curves suggest the existence of natural groupings of topological regimes across different years, opening perspectives for future analyses based on functional

Table 1: Summary of topological indicators (H_0) describing the spatial structure of dengue cases in Recife (2015–2024).

Year	N	$\varepsilon_{\text{crit}}$ (m)	$ C_{\text{max}} _{\varepsilon=300}$	$N_{\text{comp}}(300)$	$N_{\text{mid}}^{\text{max}}$	$\varepsilon_{\text{collapse}}$ (m)
2015	6165	220	5353	47	56	220
2016	4969	240	3744	52	39	240
2017	1225	410	73	224	11	410
2018	1270	390	88	210	16	410
2019	2647	450	1313	113	19	310
2020	1416	500	259	188	12	500
2021	3448	260	2498	65	39	260
2022	1338	420	74	188	20	420
2023	1670	450	200	174	19	450
2024	3636	280	2544	55	40	280

clustering or distance measures between connectivity curves.

4.2. Spatial connectivity regimes and epidemiological interpretation

The results reveal the existence of distinct spatial connectivity regimes over the analyzed period, reflecting profound structural differences in the spatial organization of dengue transmission. Such regimes are not directly inferable from traditional incidence metrics, density maps, or isolated local spatial autocorrelation analyses, as they emerge from the multiscale dynamics of connectivity among reported cases.

Years associated with intense epidemic outbreaks, such as 2015, 2016, 2021, and 2024, exhibit reduced values of $\varepsilon_{\text{crit}}$ and $\varepsilon_{\text{collapse}}$, on the order of 220–280 m, indicating early collapse of spatial connectivity. In these years, the largest connected component concentrates more than 70% of reported cases at spatial scales below 300 m, characterizing a highly concentrated spatial organization of transmission.

In contrast, years of lower epidemic intensity, such as 2017, 2018, and 2022, remain fragmented across the entire range of analyzed scales. These years display elevated values of $\varepsilon_{\text{crit}}$, close to or exceeding 390 m, reduced sizes of the largest component at $\varepsilon = 300$ m, and a large number of connected components even at larger scales, indicating a regime of diffuse spatial transmission marked by the persistence of multiple small and weakly connected clusters.

Between these extremes, the years 2019 and 2023 define an intermediate regime, characterized by the prolonged coexistence of multiple medium-sized components along the filtration, followed by a relatively late collapse of spatial connectivity. This pattern suggests a multifocal transmission process, in which different ur-

ban regions contribute simultaneously to the spatial dynamics before the consolidation of a dominant structure.

The year 2020 stands out as an atypical case. Despite presenting a substantial number of reported cases, its topological signature differs markedly from that of classical epidemic years. Both $\varepsilon_{\text{crit}}$ and $\varepsilon_{\text{collapse}}$ occur only at large spatial scales, close to 500 m, and at $\varepsilon = 300$ m the largest component contains less than 20% of the reported cases. This result highlights that high incidence does not necessarily imply high spatial concentration, an aspect not captured by analyses based solely on case counts or density maps.

Taken together, these results demonstrate that the topological analysis of spatial connectivity among dengue cases enables the identification of structural transitions in transmission regimes over time, revealing patterns of concentration, diffusion, and multifocality that remain invisible to traditional spatial approaches. In this context, zero-dimensional persistent homology acts as a multiscale geometric marker of dominant component formation, providing a solid basis for deeper physical interpretations developed in the following section.

5. Percolation analysis of spatial connectivity

To deepen the physical interpretation of the spatial patterns identified through zero-dimensional persistent homology (H_0), we analyze the spatial connectivity of dengue cases from the perspective of geometric percolation theory. This framework allows the organization of georeferenced cases to be interpreted as a continuous process of component coalescence driven by the spatial scale ε . Let $N(\varepsilon)$ denote the number of connected components of the Vietoris–Rips complex constructed from the metric coordinates of dengue cases. For $\varepsilon = 0$, each case forms an isolated component; as ε increases, spatially proximate cases become connected,

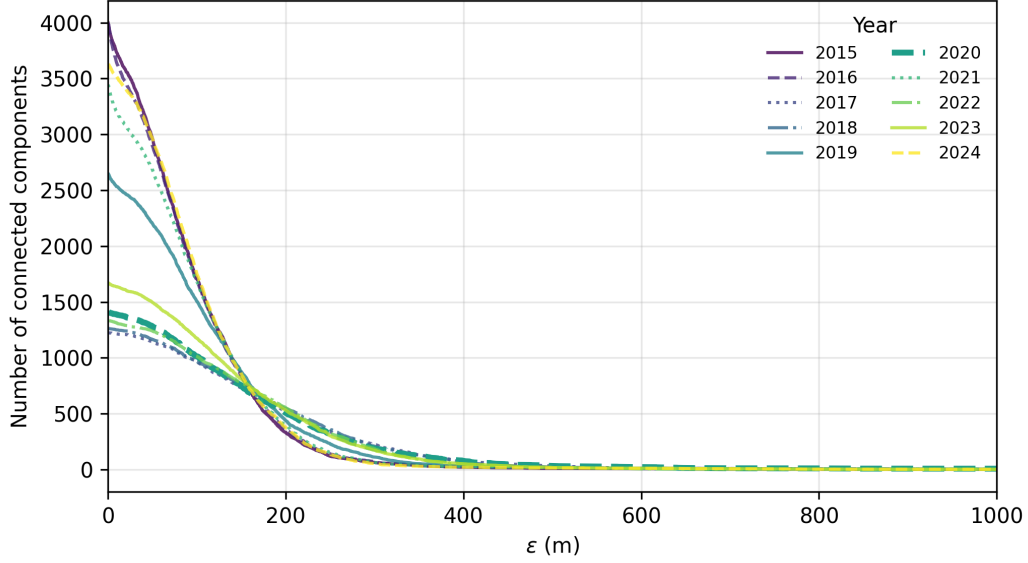


Figure 1: Global fusion curves $N(\varepsilon)$ for the zero-dimensional persistent homology of dengue cases in Recife (2015–2024), restricted to $\varepsilon \leq 1$ km. Years with intense outbreaks exhibit rapid component coalescence at short spatial scales, while milder years show gradual and diffuse percolation behavior.

leading to the progressive merging of components and the eventual emergence of a giant connected component. The curve $N(\varepsilon)$ therefore provides a multiscale description of the spatial connectivity structure of the epidemic field. Figure 1 shows the global fusion curves for all years between 2015 and 2024, restricted to epidemiologically plausible spatial scales ($\varepsilon \leq 1$ km). Despite substantial interannual variation in the total number of cases, the curves exhibit well-defined percolative signatures that allow direct comparison between different spatial regimes. Years associated with intense dengue outbreaks display a rapid decay of $N(\varepsilon)$ at short spatial scales, indicating early formation of a giant component and characterizing a regime of fast percolation. Conversely, years with lower epidemic intensity show a gradual decrease of $N(\varepsilon)$ across a wide range of scales, reflecting persistent spatial fragmentation and the absence of a sharp percolation transition.

The percolative interpretation becomes particularly transparent when the global curves are contrasted with the explicit spatial distribution of connected components. Figure 2 presents spatial maps of the connected clusters at the corresponding critical percolation scale ε^* for two representative years.

These maps confirm that rapid percolation is associated with spatially compact and strongly connected urban clusters, whereas delayed percolation corresponds to diffuse, multifocal transmission patterns.

6. Percolation-based topological metrics and epidemic intensity

While persistent homology provides a detailed multiscale characterization of spatial connectivity, its information can be synthesized into scalar observables inspired by percolation theory. Such metrics condense the geometry of the fusion process into interpretable quantities that capture the speed and abruptness of spatial cluster coalescence, enabling direct comparison across years and establishing a link between spatial organization and epidemic intensity.

6.1. Critical percolation scale

We define the *critical percolation scale* ε^* as the spatial scale at which the rate of component merging reaches its maximum. Operationally, ε^* corresponds to the value of ε that maximizes the discrete derivative $-\Delta N/\Delta \varepsilon$ along the filtration.

From a physical perspective, ε^* represents the characteristic distance at which initially local clusters rapidly coalesce into a global connected structure. Smaller values of ε^* indicate faster spatial percolation and a higher degree of spatial concentration of reported cases.

6.2. Global percolation index

To summarize the overall percolation behavior into a single scalar quantity, we define the *global percolation*

Dengue spatial clusters in Recife (2015) at $\epsilon = 140$ m Dengue spatial clusters in Recife (2020) at $\epsilon = 210$ m

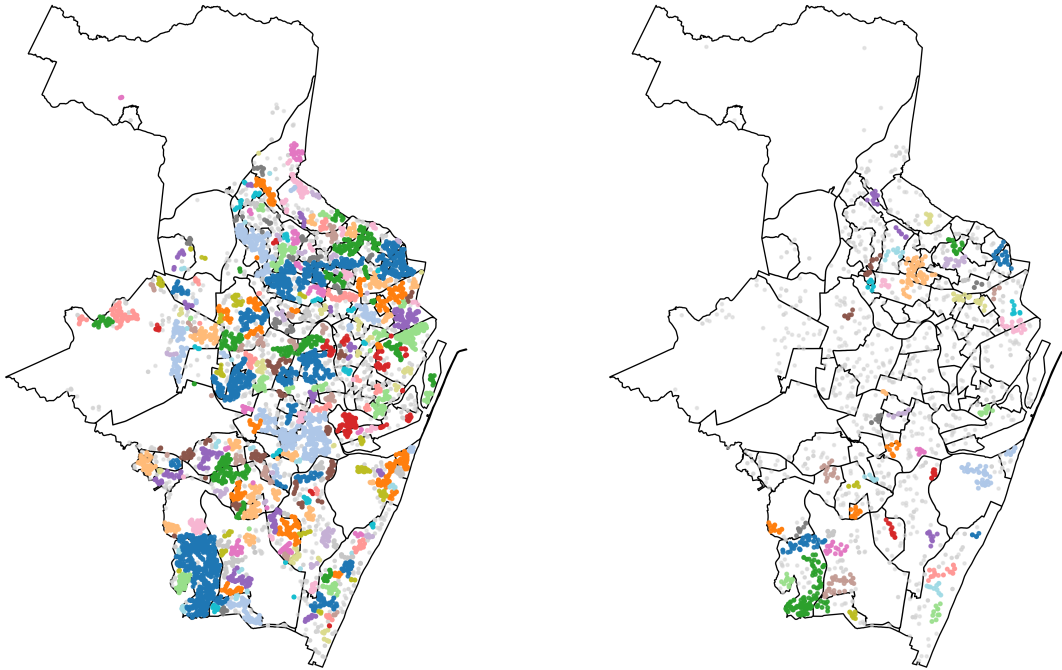


Figure 2: Spatial distribution of connected components of dengue cases in Recife at the critical percolation scale ϵ^* . Left: 2015 ($\epsilon^* = 140$ m), characterized by early emergence of large, compact clusters. Right: 2020 ($\epsilon^* = 210$ m), exhibiting fragmented and spatially dispersed components. Colors indicate distinct connected components.

index as

$$P = \int_0^{\epsilon_{\max}} \frac{N(\epsilon)}{N(0)} d\epsilon, \quad (1)$$

which is numerically approximated along the discrete filtration.

This quantity corresponds to the area under the normalized fusion curve and provides an aggregate measure of the persistence of spatial fragmentation across scales. Smaller values of P indicate a rapid collapse of spatial connectivity, whereas larger values reflect slow, diffuse, or weakly connected percolation dynamics.

6.3. Correlation with epidemic incidence

To assess the epidemiological relevance of the percolation-based metrics, we examined their association with annual dengue incidence. Spearman rank correlation analysis reveals a strong and statistically significant negative relationship between incidence and both observables:

$$\rho(\epsilon^*, I) \approx -0.99, \quad \rho(P, I) \approx -0.98, \quad p < 10^{-3}.$$

These results indicate that years with higher epidemic intensity tend to exhibit faster spatial percolation and reduced persistence of spatial fragmentation.

6.4. Physical interpretation and implications

These results demonstrate that the spatial percolation properties of dengue case distributions encode meaningful information about epidemic severity. The rapid emergence of a giant connected component at short spatial scales reflects highly concentrated urban transmission, whereas delayed percolation is associated with diffuse or multifocal spatial dynamics.

Importantly, the metrics ϵ^* and P are derived exclusively from the spatial geometry of the data, without imposing explicit transmission models or assumptions regarding vector behavior. As such, they provide interpretable, data-driven, and physically motivated descriptors of epidemic structure, with potential applications in spatial surveillance and early warning systems.

Conjectura 1. *Empirical rigidity of urban percolation*
In spatial processes constrained by an urban support,

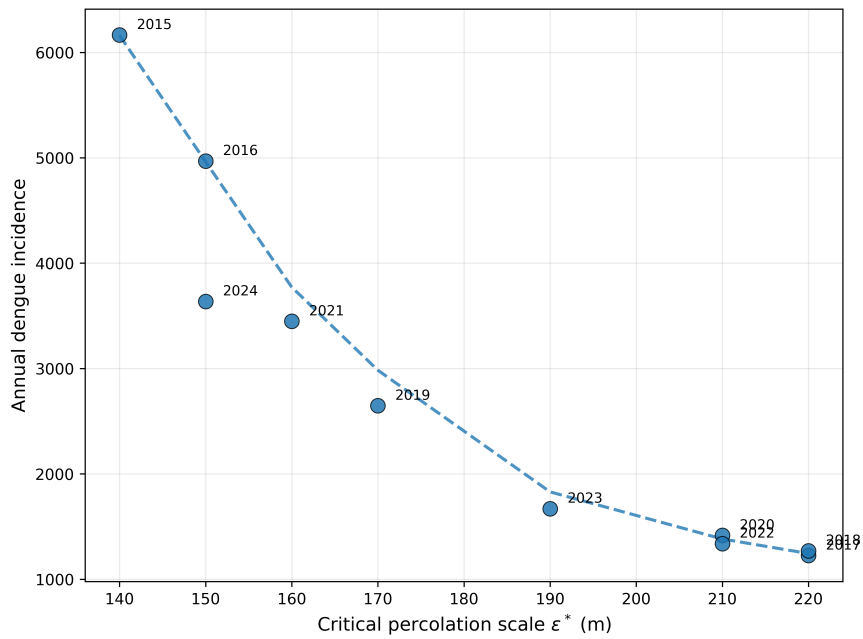


Figure 3: Relationship between the critical percolation scale ϵ^* and annual dengue incidence in Recife (2015–2024). Lower values of ϵ^* indicate faster spatial percolation and are strongly associated with higher incidence levels. The dashed curve represents a LOWESS smoothing shown only as a guide to the eye.

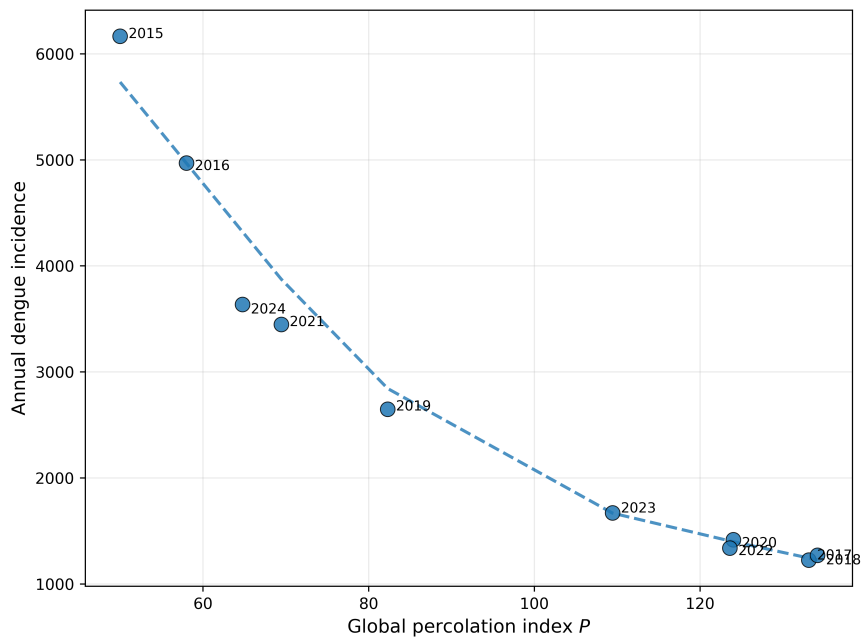


Figure 4: Relationship between the global percolation index P and annual dengue incidence in Recife (2015–2024). Smaller values of P , corresponding to more rapid spatial percolation, are associated with increased epidemic intensity. The dashed curve represents a LOWESS smoothing shown only as a guide to the eye.

signatures of rapid percolation characterized by small values of ε^* and steep fusion curves cannot be reproduced by null models that preserve only the underlying spatial support. Such signatures therefore reflect non-random spatial organization associated with structural mechanisms beyond simple urban geometry.

This conjecture is supported by the empirical evidence presented in this work and suggests that percolation-based topological observables may act as robust detectors of emergent spatial structure in finite urban systems.

7. Geometric Structure of Epidemic Connectivity

The spatial dynamics of dengue transmission in urban environments constitute a finite complex system in which local interactions between hosts and vectors generate emergent collective patterns of connectivity. Although density maps and aggregated statistics provide information regarding epidemic intensity, such descriptors do not explicitly capture the underlying structural organization of spatial connectivity driving the transmission process.

In this work, we model the annual distribution of dengue cases as an empirical realization of a finite spatial point process and investigate its multiscale connectivity structure using tools from computational algebraic topology and geometric percolation theory.

7.1. Geometric Representation of the Data

Let

$$\mathcal{D}_y = \{x_i\}_{i=1}^{N_y} \subset \mathbb{R}^2$$

denote the set of spatial coordinates of the N_y reported cases in year y , represented in the UTM coordinate system (meters), ensuring Euclidean metric consistency.

The spatial distance between two cases is defined as

$$d_{ij} = \|x_i - x_j\|.$$

This representation initially disregards administrative partitions, treating the data as a point cloud embedded in a continuous urban domain. Such a choice avoids spatial aggregation bias (the Modifiable Areal Unit Problem, MAUP) and enables a purely geometric analysis of connectivity.

7.2. Vietoris–Rips Filtration

To investigate multiscale connectivity, we employ the Vietoris–Rips filtration. For each scale parameter $\varepsilon \geq 0$, we define the simplicial complex

$$\mathcal{VR}_\varepsilon(\mathcal{D}_y) = \{\sigma \subset \mathcal{D}_y \mid d_{ij} \leq \varepsilon \ \forall i, j \in \sigma\}.$$

In practice, we focus on zero-dimensional homology, which describes the number of connected components of the associated geometric graph. We define

$N_y(\varepsilon)$ = number of connected components in $\mathcal{VR}_\varepsilon(\mathcal{D}_y)$.

For $\varepsilon = 0$, we have $N_y(0) = N_y$, since each point forms an isolated component. As ε increases, components progressively merge until the eventual emergence of a dominant connected component.

The structural transition is characterized by the empirical critical scale

$$\varepsilon_y^* = \arg \max_{\varepsilon} \left(-\frac{dN_y}{d\varepsilon} \right),$$

numerically estimated as the point of largest discrete negative variation of the curve $N_y(\varepsilon)$.

Physically, ε_y^* represents the spatial scale at which the most abrupt component coalescence occurs, that is, the point of maximal structural reorganization of urban connectivity.

Large values of ε^* indicate that a broader spatial radius is required to achieve global connectivity, suggesting a fragmented regime. Conversely, small values indicate early formation of a dominant component, suggesting spatial concentration of cases.

Beyond the critical scale, we define the global percolation index

$$P_y = \int_0^{\varepsilon_{\max}} \frac{N_y(\varepsilon)}{N_y(0)} d\varepsilon.$$

This quantity measures the overall persistence of fragmentation across spatial scales.

High values of P_y indicate that the network remains fragmented over a wide range of scales, whereas low values indicate rapid consolidation of connectivity.

While ε^* captures the transition point, P_y summarizes the global intensity of fragmentation.

7.3. Interpretation as a Finite Percolation System

It is important to emphasize that the system under investigation is finite and non-stationary. Unlike classical percolation on infinite lattices, we analyze an empirically bounded spatial realization.

Nevertheless, the behavior of the curve $N_y(\varepsilon)$ exhibits qualitative signatures analogous to percolation transitions in random geometric graphs: a fragmented phase,

a rapid coalescence regime, and the emergence of a dominant component.

However, as demonstrated in subsequent sections, the observed organization cannot be explained solely by generic geometric properties, requiring validation against structured null models.

The choice of zero-dimensional homology is deliberate. In urban epidemiological systems, the spatial connectivity of infection foci constitutes a macroscopic variable relevant to collective propagation.

Rather than explicitly modeling vector dynamics, this approach extracts structural invariants directly from empirical geometry, enabling:

- Interannual comparison independent of absolute incidence;
- Identification of distinct structural regimes;
- Multiscale analysis without arbitrary spatial partitioning;
- Integration with complex systems theory and geometric percolation.

This formulation establishes the fundamental geometric framework upon which we introduce, in subsequent sections, temporal constraints and structured null model validation.

8. Spatiotemporal Structure: Sliding Windows and Causal Filtration

The purely spatial representation introduced in the previous section captures the aggregated annual geometry of the epidemic. However, dengue transmission is intrinsically spatiotemporal: epidemiologically plausible connections depend not only on spatial proximity but also on temporal compatibility between cases.

In this section, we introduce two distinct strategies for incorporating the temporal dimension and analyze their structural implications.

Let

$$\mathcal{D}_y = \{(x_i, t_i)\}_{i=1}^{N_y},$$

where $x_i \in \mathbb{R}^2$ denotes the spatial position (UTM coordinates) and $t_i \in [0, T_y]$ the time in days within year y .

We define the temporal separation between two cases as

$$\Delta t_{ij} = |t_i - t_j|.$$

We fix a temporal horizon $\Delta T > 0$ (in days), interpreted as an epidemiologically plausible interaction window mediated by the vector.

We investigate two distinct constructions.

8.1. Model A: Sliding Temporal Windows

In the window-based model, the annual dataset is partitioned into independent temporal subsets.

For a fixed duration ΔT , we define windows

$$W_k = \{(x_i, t_i) \in \mathcal{D}_y \mid t_i \in [\tau_k, \tau_k + \Delta T)\},$$

where τ_k traverses the year with fixed step size.

Within each window W_k , we apply a purely spatial Vietoris–Rips filtration:

$$\mathcal{VR}_\varepsilon(W_k) = \{\sigma \subset W_k \mid \|x_i - x_j\| \leq \varepsilon \forall i, j \in \sigma\}.$$

Let $N_k(\varepsilon)$ denote the number of connected components in window k .

The annual averaged curve is defined as

$$N_{\text{window}}(\varepsilon) = \frac{1}{K} \sum_{k=1}^K N_k(\varepsilon).$$

Structural Interpretation. This model preserves local spatial structure within each temporal interval but eliminates structural continuity across distinct windows. Components that could potentially connect through temporal chaining are artificially disconnected.

From a complex systems perspective, the window-based model performs a temporal coarse-graining with periodic structural reinitialization.

8.2. Model B: Weak Causal Filtration

In the weak causal model, the full annual structure is preserved, but connections are allowed only when spatially and temporally compatible.

We define the masked metric

$$\tilde{d}_{ij}^{(\Delta T)} = \begin{cases} \|x_i - x_j\|, & \text{if } \Delta t_{ij} \leq \Delta T, \\ +\infty, & \text{otherwise.} \end{cases}$$

The causal filtration is then defined as

$$\mathcal{VR}_\varepsilon^{\text{causal}} = \{\sigma \subset \mathcal{D}_y \mid \tilde{d}_{ij}^{(\Delta T)} \leq \varepsilon \forall i, j \in \sigma\}.$$

We denote by $N_{\text{causal}}(\varepsilon)$ the associated number of connected components.

Structural Interpretation. Unlike the window-based model, no artificial partitioning of the year is introduced. Connections may occur between any two cases provided they satisfy the temporal constraint ΔT .

This allows the formation of spatiotemporal chains that propagate across the entire year through successive local linkages.

The term ‘‘causal’’ is used in a structurally weak sense: we do not explicitly model vector dynamics, but we impose epidemiologically plausible temporal coherence.

8.3. Fundamental Structural Difference

The two constructions differ fundamentally:

- The window-based model fragments annual structural continuity.
- The causal model preserves global connectivity subject to local temporal constraints.

In terms of dynamic geometric graphs:

- The window-based model corresponds to a sequence of independent graphs.
- The causal model corresponds to a single temporally constrained spatiotemporal graph.

This distinction is central. If the observed organization arises solely from local spatial density, both models should produce similar structural signatures.

If genuine spatiotemporal chaining exists, the causal model is expected to exhibit:

- a smaller critical scale ε^* ;
- a lower global percolation index P ;
- stronger contrast relative to null models that destroy spatiotemporal correlation.

The next section formalizes the null models employed to evaluate this hypothesis.

9. Structural Comparison Between Filtering Pipelines and Validation via Null Models

In this section, we investigate the spatiotemporal organization of epidemic connectivity under two distinct filtering schemes:

1. Sliding temporal window filtration;

2. Weak causal filtration with global temporal constraint.

The analysis is conducted under a fixed temporal horizon $\Delta T = 14$ days, chosen to reflect an epidemiologically plausible scale of infectious chaining.

Let the annual dataset be defined as

$$\mathcal{D}_y = \{(x_i, t_i)\}_{i=1}^{N_y},$$

where $x_i \in \mathbb{R}^2$ denotes the spatial position (UTM coordinates) and t_i the time in days within year y .

Spatial distance is defined by

$$d_{ij} = \|x_i - x_j\|.$$

The structural metrics considered are:

- the critical scale ε^* (largest discrete drop of $N(\varepsilon)$);
- the global percolation index

$$P = \int \frac{N(\varepsilon)}{N(0)} d\varepsilon.$$

9.1. Filtering Pipelines

Sliding Window Filtration

The annual dataset is partitioned into independent windows of width ΔT :

$$W_k = \{(x_i, t_i) \in \mathcal{D}_y \mid t_i \in [\tau_k, \tau_k + \Delta T)\}.$$

Within each window, a purely spatial Vietoris–Rips filtration is applied, producing $N_k(\varepsilon)$.

The aggregated curve is defined as

$$N_{\text{window}}(\varepsilon) = \frac{1}{K} \sum_{k=1}^K N_k(\varepsilon).$$

This pipeline preserves local spatial structure but eliminates inter-window structural continuity.

Weak Causal Filtration

Define temporal separation as

$$\Delta t_{ij} = |t_i - t_j|.$$

The masked metric is defined by

$$\tilde{d}_{ij}^{(\Delta T)} = \begin{cases} d_{ij}, & \text{if } \Delta t_{ij} \leq \Delta T, \\ +\infty, & \text{otherwise.} \end{cases}$$

The causal filtration is constructed using $\tilde{d}_{ij}^{(\Delta T)}$, retaining the complete annual dataset.

This scheme preserves global structural continuity across the year, removing only temporally incompatible connections.

9.2. Null Models

Two complementary null models were employed.

Null Model A — Temporal Permutation

Time labels are randomly permuted:

$$t_i^{(\pi)} = t_{\pi(i)},$$

preserving the marginal spatial and temporal distributions while destroying spatiotemporal correlation.

A total of 500 permutations were performed per year.

Null Model B — Inhomogeneous Spatial Resampling

The estimated spatial intensity $\lambda(x)$ is preserved, and a new independent sample of N_y points is generated according to this intensity.

This model maintains global urban heterogeneity but removes specific relational chaining.

9.3. Comparative Results for $\Delta T = 14$ Days

Causal Pipeline Under Two Null Models

Table 2: Causal pipeline ($\Delta T = 14$ days) compared to two null models.

Year	ε^*	P	$p_A(\varepsilon^*)$	$p_B(\varepsilon^*)$	$p_B(P)$
2015	103.76	153.80	0.446	0.010	0.023
2016	79.32	195.31	0.066	0.000	0.010
2017	582.71	578.99	0.888	0.570	0.000
2018	499.62	572.50	0.794	0.347	0.000
2019	113.53	322.78	0.004	0.000	0.000
2020	250.38	491.72	0.162	0.060	0.000
2021	191.73	259.02	0.208	0.423	0.000
2022	455.64	540.61	0.890	0.233	0.000
2023	445.86	478.09	0.642	0.293	0.000
2024	211.28	243.36	0.924	0.453	0.000

We observe that:

- Under temporal permutation (Null A), statistical significance varies across years;
- Under the inhomogeneous spatial model (Null B), the global index P remains systematically significant;
- The critical scale ε^* is partially explained by spatial heterogeneity, but not fully.

These results indicate that the observed structure cannot be attributed solely to urban density patterns.

Table 3: Sliding window pipeline compared to the temporal permutation null model ($\Delta T = 14$ days).

Year	ε^*	P	$p(\varepsilon^*)$	$p(P)$
2015	100.84	276.05	0.592	1.000
2016	100.84	329.57	0.528	1.000
2017	605.04	942.03	0.600	0.004
2018	789.92	971.66	0.858	0.824
2019	100.84	552.01	0.000	1.000
2020	605.04	763.14	0.982	1.000
2021	100.84	446.95	0.252	1.000
2022	689.08	904.94	0.780	0.048
2023	487.39	827.49	0.412	0.078
2024	201.68	447.78	0.226	0.992

Window-Based Pipeline Under Temporal Permutation

Comparatively, the window-based pipeline exhibits reduced discriminative power under temporal randomization.

Annual fragmentation diminishes statistical sensitivity to global spatiotemporal structural coherence.

The results suggest that:

- A portion of the observed organization arises from underlying urban spatial heterogeneity;
- However, the global percolation index remains significantly distinct even under spatially inhomogeneous control;
- The causal filtration preserves multiscale structural coherence that is not captured by the window-based model.

These findings indicate that the identified organization constitutes a robust structural property of the urban transmission system, rather than a mere artifact of density effects or temporal randomness.

10. Morphology of the Percolation Transition: Structural Shape Metrics

Classical percolation metrics — the critical scale ε^* and the integrated index P — capture, respectively, the transition point and the aggregated intensity of connectivity. However, these quantities do not distinguish different *transition morphologies*, that is, distinct functional shapes of the merging curve $N(\varepsilon)$.

Empirical observations indicate that years with markedly different epidemic intensities may exhibit similar values of ε^* , yet display globally distinct concavity patterns in their merging curves. In particular, we

identify two qualitative regimes: (i) abrupt transitions, characterized by strong global upward concavity and associated with rapid structural collapse; and (ii) smooth, diffuse transitions, characterized by reduced or negative global concavity and associated with progressive connectivity.

To quantify these structural differences, we introduce a set of metrics derived from the discrete geometry of the merging curve.

Let $N(\varepsilon_k)$ denote the curve evaluated on an increasing grid $\{\varepsilon_k\}_{k=1}^K$. We define the discrete second difference:

$$\kappa_k = N(\varepsilon_{k+1}) - 2N(\varepsilon_k) + N(\varepsilon_{k-1}), \quad k = 2, \dots, K-1.$$

The global mean curvature is then defined as

$$\bar{\kappa} = \frac{1}{K-2} \sum_{k=2}^{K-1} \kappa_k.$$

Positive values of $\bar{\kappa}$ indicate average upward concavity, characterizing rapid structural collapse. Negative values indicate gradual transitions.

To evaluate how merging intensity is distributed across scales, we consider the discrete variations

$$\Delta_k = |N(\varepsilon_{k+1}) - N(\varepsilon_k)|.$$

We define the normalized distribution

$$p_k = \frac{\Delta_k}{\sum_{j=1}^{K-1} \Delta_j},$$

and the structural entropy

$$H = - \sum_{k=1}^{K-1} p_k \log p_k.$$

Low entropy values indicate transitions concentrated at specific scales, whereas high entropy reflects merging distributed across multiple scales.

Let ε^* denote the critical scale estimated via the maximum discrete derivative. We further define the accumulated areas before and after the critical point:

$$A_{\text{before}} = \int_0^{\varepsilon^*} N(\varepsilon) d\varepsilon, \quad A_{\text{after}} = \int_{\varepsilon^*}^{\varepsilon_{\text{max}}} N(\varepsilon) d\varepsilon,$$

and the structural asymmetry ratio

$$\mathcal{A} = \frac{A_{\text{before}}}{A_{\text{after}}}.$$

Large values of \mathcal{A} indicate early formation of a dominant component.

Finally, we define the normalized structural intensity index

$$S_{\text{norm}} = \frac{1}{N(0)} \int_0^{\varepsilon_{\text{max}}} N(\varepsilon) d\varepsilon,$$

which measures the overall persistence of fragmentation across scales.

Table 4 reports the values obtained for the causal model with $\Delta T = 14$ days.

Table 4: Structural shape metrics of the percolation transition (causal model, $\Delta T = 14$ days).

Year	S_{norm}	$\bar{\kappa}$	H	\mathcal{A}
2015	0.0415	3.3644	3.9243	2.7000
2016	0.0393	2.7203	4.0683	2.8182
2017	0.0141	-0.0593	4.6622	2.5385
2018	0.0138	-0.0169	4.6712	2.4750
2019	0.0219	0.2712	4.4774	2.6190
2020	0.0175	0.0085	4.6607	3.0357
2021	0.0262	0.7119	4.3071	2.8000
2022	0.0157	-0.0593	4.6907	2.3250
2023	0.0150	0.0085	4.6802	2.5152
2024	0.0248	0.3220	4.3189	2.5882

The results reveal two structurally distinct regimes. Years such as 2015 and 2016 exhibit strongly positive mean curvature and lower structural entropy, characterizing abrupt transitions and spatially concentrated organization. In contrast, years such as 2017, 2018, and 2022 display mean curvature near zero or negative and elevated entropy, reflecting diffuse and multifocal connectivity regimes.

This separation is not captured solely by ε^* or P , but emerges clearly from the morphology of the merging curve.

From the perspective of complex systems physics, these findings suggest that intense outbreaks correspond to regimes of more rapid structural consolidation of the spatiotemporal network, whereas low-intensity years operate under a fragmented dynamical regime.

11. Limitations and Interpretative Scope

Although the results indicate robust structural organization under multiple null models and temporal horizons, the adopted framework presents conceptual and methodological limitations that must be explicitly acknowledged.

First, the model is fundamentally geometric-topological. Connections are defined through spatial

proximity and temporal compatibility, but do not explicitly incorporate biological transmission mechanisms, human mobility patterns, vector heterogeneity, or socio-environmental drivers. The term “causal” employed in the spatiotemporal filtration refers solely to a minimal structural constraint of temporal coherence and does not imply mechanistic inference nor reconstruction of actual transmission chains.

Second, the analysis relies on reported case data, which are subject to underreporting, reporting delays, and potential spatial biases associated with epidemiological surveillance infrastructure. Although the temporal permutation null model preserves marginal spatial and temporal distributions, it does not fully control for latent heterogeneities related to urban accessibility or institutional reporting patterns.

A third limitation concerns parametric choices. The temporal horizon ΔT and the discretization of the spatial parameter ε influence the resolution of the percolation transition. Despite the qualitative stability observed for $\Delta T \in \{14, 21, 28\}$ days, these values reflect epidemiological plausibility rather than inferential estimates of effective transmission time.

Additionally, the global metrics ε^* and P condense connectivity dynamics into aggregated descriptors. Although we introduced morphological metrics to characterize the functional shape of the transition, these quantities do not exhaust the potential structural complexity of the system.

Finally, the analysis focuses exclusively on zero-dimensional homology, that is, component connectivity. Higher-dimensional topological structures, such as persistent cycles and spatial cavities, were not explored and may reveal additional information regarding urban fragmentation patterns.

These limitations delimit the interpretative scope of the study: the results should be understood as a structural characterization of observed spatiotemporal organization, rather than a complete mechanistic epidemiological model.

In this sense, the present work constitutes an initial step toward integrating applied topology and urban epidemiology, opening avenues for future investigations incorporating explicit transmission dynamics and higher-dimensional topological invariants.

12. Future Directions

The structural framework introduced here naturally suggests several extensions at both methodological and theoretical levels.

A first direction concerns the internal organization of the percolated regime. Once large connected components emerge, their internal architecture can be analyzed using graph-theoretic and spectral tools. Metrics such as degree heterogeneity, eigenvector centrality, communicability-based curvature, and spectral gap analysis may reveal structurally dominant nodes and spatial backbone regions within the epidemic network.

A second avenue involves controlled structural perturbations. Targeted node- or edge-removal experiments could be performed to quantify robustness of the percolation transition and to evaluate sensitivity of critical scales to localized interventions. Such experiments would establish a bridge between geometric percolation, network fragility, and structural control in urban epidemic systems.

From a topological perspective, extensions to higher-dimensional homology represent a particularly promising direction. Persistent cycles may encode spatial voids, barriers, or circulation corridors that are invisible in dimension-zero connectivity analysis. Incorporating higher-dimensional invariants could therefore enrich the structural characterization of urban transmission patterns.

Finally, the integration of the present geometric-topological framework with dynamical epidemic models constitutes a natural next step. Embedding mechanistic SIR-type dynamics on top of empirically derived structural networks would allow investigation of how topology constrains or amplifies disease propagation.

Together, these directions indicate that the present study should be viewed not as an endpoint, but as a structural foundation for a broader program connecting topology, network theory, and epidemiological dynamics.

13. Conclusion

We investigated the spatial organization of dengue transmission in Recife, Brazil, over a ten-year period using geometric percolation and topological data analysis. Modeling reported cases as spatial point clouds, we analyzed their zero-dimensional persistent homology to characterize the multiscale evolution of spatial connectivity without imposing administrative boundaries or explicit mechanistic assumptions.

The results reveal well-defined percolation signatures across epidemic years, allowing identification of distinct structural regimes ranging from diffuse, multifocal configurations to rapidly coalescing, spatially concentrated patterns. Importantly, years with compara-

ble incidence levels exhibit markedly different transition morphologies, indicating that epidemic magnitude alone does not determine spatial organization.

By introducing a weak causal filtration that enforces temporal compatibility, we showed that preserving space–temporal coherence significantly enhances structural discrimination relative to sliding-window constructions. Comparisons against temporally permuted null ensembles demonstrate that the causal framework captures organization that cannot be explained by random temporal reshuffling alone.

Beyond classical percolation descriptors, we introduced morphological metrics of the fusion curve, revealing two qualitatively distinct transition classes: abrupt, low-entropy consolidation regimes and diffuse, high-entropy fragmentation regimes. These structural distinctions remain stable under moderate variations of the temporal horizon, indicating robustness of the detected organization.

A notable anomaly was observed in 2020, where substantial case counts did not translate into rapid structural consolidation, suggesting that large-scale perturbations in urban mobility can reshape spatial connectivity independently of incidence magnitude.

More broadly, this study illustrates how tools from statistical physics, percolation theory, and algebraic topology can extract structural information from high-resolution epidemiological data. The proposed framework is geometry-driven, model-free, and extensible to other vector-borne diseases and complex urban systems. Rather than replacing mechanistic epidemic models, it provides a complementary structural layer that quantifies how spatial connectivity emerges and reorganizes across scales.

14. Data and Code Availability

The geocoded dengue dataset used in this study is publicly available on Zenodo [15]. The dataset comprises anonymized case locations for the municipality of Recife between 2015 and 2024 and was processed to ensure spatial consistency in projected metric coordinates.

All scripts used for data preprocessing, construction of Vietoris–Rips complexes, computation of H_0 persistent homology, extraction of percolation curves $N(\varepsilon)$, and generation of figures are available in an open GitHub repository [15].

References

- [1] C. Barcellos and P. C. Sabroza, “Socio-environmental determinants of the dengue fever epidemic in Brazil,” *Cadernos de Saúde Pública*, vol. 17, pp. 385–393, 2001.
- [2] M. G. Teixeira, M. C. N. Costa, F. Barreto, and E. Mota, *Dengue: twenty-five years since its reemergence in Brazil*, Cadernos de Saúde Pública, 25(Suppl 1), S7–S18, 2009.
- [3] N. A. Honório et al., “Dispersal of *Aedes aegypti* and *Aedes albopictus* in an urban endemic dengue area in Brazil,” *Memórias do Instituto Oswaldo Cruz*, vol. 98, no. 2, pp. 191–198, 2003.
- [4] M. J. Keeling and P. Rohani, *Modeling Infectious Diseases in Humans and Animals*, Princeton University Press, 2008.
- [5] H. Edelsbrunner, D. Letscher, and A. Zomorodian, “Topological persistence and simplification,” in *Proc. 41st IEEE FOCS*, pp. 454–463, 2000.
- [6] A. Zomorodian and G. Carlsson, “Computing persistent homology,” *Discrete & Computational Geometry*, vol. 33, no. 2, pp. 249–274, 2005.
- [7] F. Chazal et al., “An introduction to topological data analysis,” *arXiv:1710.04019*, 2016.
- [8] D. Stauffer and A. Aharony, *Introduction to Percolation Theory*, 2nd ed., Taylor & Francis, 1994.
- [9] M. Penrose, *Random Geometric Graphs*, Oxford University Press, 2003.
- [10] S. N. Dorogovtsev, A. V. Goltsev, and J. F. F. Mendes, “Critical phenomena in complex networks,” *Rev. Mod. Phys.*, vol. 80, pp. 1275–1335, 2008.
- [11] M. Barthélemy, “Spatial networks,” *Physics Reports*, vol. 499, pp. 1–101, 2011.
- [12] M. Kramár et al., “Persistence of force networks in compressed granular media,” *Phys. Rev. E*, vol. 87, 042207, 2013.
- [13] S. Bhatt, D. Kumar, and A. Singh, “Topological methods in spatial epidemiology,” *Scientific Reports*, vol. 13, 2043, 2023.
- [14] M. R. Cayo and T. O. Talbot, “Positional error in automated geocoding of residential addresses,” *Int. J. Health Geographics*, vol. 2, no. 1, 2003.

- [15] Ferreira dos Santos, M. and Rodrigues de Melo, A., *Dengue Cases in Recife, Brazil (2015–2024)* [Data set], Zenodo, 2025.
- [16] Ferreira dos Santos, M., *Dengue Percolation and TDA Analysis – Code Repository*, GitHub, 2025.